SMALL-SCALE CHARACTERIZATION OF SHOCK SENSITIVITY FOR VARIOUS NON-IDEAL EXPLOSIVES BASED ON DETONATION FAILURE BEHAVIOR

A Thesis

Submitted to the Faculty

of

Purdue University

by

Dakota G. Scott

In Partial Fulfillment of the

Requirements for the Degree

of

Master of Science in Mechanical Engineering

August 2019

Purdue University

West Lafayette, Indiana

THE PURDUE UNIVERSITY GRADUATE SCHOOL
STATEMENT OF THESIS APPROVAL

Dr. Steven Son, Chair

School of Mechanical Engineering

Dr. Metin Ornek

School of Mechanical Engineering

Dr. Wayne Chen

School of Aeronautics and Astronautics

Approved by:

Dr. Jay Gore

Head of the School Graduate Program

To the Lord and loved ones.

ACKNOWLEDGMENTS

I would like to thank my advisor, Steven Son, whose guidance marked the path forward and whose expertise provided me with the tools I would need to see that path to the end. His contributions were instrumental in the completion of this work. I could not be more grateful for the time he has invested in my academic career and the connections I have made through him which have shaped the future of my professional career.

Additional thanks to the many faculty and staff members who have assisted me in my time here. In particular Tim Manship, Metin Ornek, and Emry Gunduz. Their advice was always an invaluable resource.

Nick Cummock was my predecessor on this project and I am proud to call him a mentor. He was always the sounding board for my ideas. The knowledge he passed on to me played no small role in my academic development and the timely completion of this research. In addition, I would like to thank my fellow students Christian Sorensen and Vasant Vuppuluri who were also amazing resources as well as the keepers of the magazine keys. No matter the hour, they would make their way out to the lab just so I could perform my experiments.

I can say in all earnest that the friendships I have developed here at Zucrow Labs are worth just as much to me as the academic accomplishments. They helped make every long night and failed experiment worth it. It has been a gratifying spectacle watching these extraordinary men and women march tirelessly up the hill of science with noble emulation. I am honored to have been able to stand alongside these brilliant individuals during this endeavor. I wish them all the best of luck, if only as a gesture because I know they will not need it. I cannot convey the overwhelming excitement I have to see what glory and acclaim awaits them as they cross the sea of years.

I would like to thank my family for their unwavering love and support, but my acknowledgement of the role they have played goes far beyond that. Anything by my hands is nothing if not a reflection of their influence and an homage to their virtue.

Finally, it is by God's unending grace that I have made it this far. I consider myself very blessed to have been met with such success working toward the career I have dreamed of since childhood.

This material is based upon work supported by the U.S. Department of Homeland Security, Science and Technology Directorate, Office of University Programs, under Grant Award No. 2013-ST-061-ED0001. The views and conclusions contained in this document are those of the authors and should not be interpreted as necessarily representing the official policies, either expressed or implied, of the U.S. Department of Homeland Security.

TABLE OF CONTENTS

LIST OF TABLES

LIST OF FIGURES

ABSTRACT

Scott, Dakota G. MSME, Purdue University, August 2019. Small-Scale Characterization of Shock Sensitivity for Various Non-Ideal Explosives Based on Detonation Failure Behavior. Major Professor: Steven F. Son.

The plethora of potential homemade explosive (HME) formulations combined with the fact they often exhibit large critical diameters make them expensive to characterize with traditional large-scale tests. A relatively new method for small-scale characterization was investigated using non-ideal explosive charges consisting of ammonium nitrate (AN) and various fuels. This optical characterization technique utilizes the rate of reaction wave velocity decay in the failing detonations of sub-critical diameter charges as a metric for the shock sensitivity of an explosive. The conditions for detonation initiation and failure have long been used to investigate shock sensitivity (critical diameter, gap tests, run-to-detonation experiments); however, the failure regime still remains largely unexplored. The utility of this small-scale characterization technique lies in its ability to determine the relative shock sensitivity of explosive with minimal material and tests while simultaneously providing transient velocity data for potential use in modeling efforts. In this work, high speed imaging was used and analyzed to determine rates of reaction wave velocity decay in the AN-fuel samples. Among the fuels tested with AN were diesel (ANFO), nitromethane (ANNM), and aluminum (ANAl). It was found that nitromethane was the most effective at sensitizing the AN of the systems considered. In both ANNM and ANAl, maximum shock sensitivity occurred at fuel percentages below stoichiometric mixtures. This was speculated to be due to the competing effects of stoichiometry and hot spot criticality. Sensitivity results were compared to run-to-failure distances and published critical diameter trends and showed good agreement.

1. INTRODUCTION

Ammonium nitrate (AN) is the most widely used and consumed ammonium salt with an annual worldwide production that exceeds 57.5 million tons [1]. While it has seen use in many military and civilian blasting applications due to its properties as an explosive oxidizer, it is primarily used as an inorganic fertilizer. The invention of the Haber process allowed for the large-scale commercial production of AN in the early 1900s and disaster followed shortly after [2]. In 1921, an industrial accident involving 450 tons of AN destroyed a manufacturing facility in Oppau, Germany. The explosion resulted in nearly 2,600 casualties and left 7,500 homeless [3]. This is only one in a long line of industrial disasters caused by AN. Others include the Texas City disaster in 1947 and the explosion at a French fertilizer company in Tolouse, France in 2001 [3]. Unfortunately, the destructive potential of AN is not restricted to industrial accidents. Its ready availability has made it popular among terrorists and terrorist groups in the manufacture of homemade explosives (HMEs) [4]. Ammonium nitrate was involved in one of the worst terrorist attacks in U.S. history. On April 19th, 1995 Timothy McVeigh detonated an HME device underneath the Murrah Building in Oklahoma City, Oklahoma. The resulting explosion killed 168 people and injured another 680. This device consisted of rental truck filled with 13 plastic barrels full of a mixture of AN and nitromethane (a common racing fuel) [5].

For these reasons it is of interest to be able to characterize the detonation properties of AN and AN-based explosives. It is necessary in order to ensure their safe handling, tailor their detonation performance, and to properly assess the security threat they pose. Characterizing these explosives is difficult in practice for two reasons. The first difficulty arises from the extremely large parameter space of variables that can affect the detonation performance of AN based explosives. Ammonium nitrate is itself detonable though highly insensitive; however, the addition of nearly any type of

fuel creates a more powerful explosive with greater sensitivity to detonation [6]. Ammonium nitrate and fuel oil (ANFO) and ammonium nitrate and aluminum (ANAl) are two of the more common AN-fuel mixtures. Ammonium nitrate is also mixed with other explosives to improve the oxygen balance and performance. Examples include AN and TNT (amatol) and AN and nitromethane (ANNM). Besides fuel type, other parameters that can have a pronounced effect on the detonation characteristics of AN are fuel percentage, particle size and morphology, initial density, the nature of confinement, and the presence of inert materials (which can be diluents such as calcium carbonate or sensitizers such as glass microballoons).

The second difficulty in conducting characterization studies with AN based explosives stems from its highly non-ideal detonation behavior. A detonation is said to behave ideally when its characteristics (velocity, temperature, pressure, etc.) match those of its theoretically predicted values. These theoretically predicted values can only be achieved by a planar detonation in an infinite diameter charge. In such a configuration, the detonation would be independent of reaction zone structure and propagated at its infinite diameter velocity D_∞ [7]. In finite diameter charges, lateral losses take place through the sides of the reaction zone and causes curvature of the detonation front. This leads to a reduction in the detonation velocity as well as the shock-jump conditions across the front (and therefore the thermodynamic state in the reaction zone). As shown in Fig. 1.1, as the diameter is reduced, so to is the ratio of energy release to lateral energy losses and the detonation performance diverges from its ideal values. Eventually the thermodynamic state behind the increasingly curved front is no longer capable of producing the energy release rate necessary to sustain a detonation. The diameter at which this happens is known as the critical diameter of the explosive (d_c) [7]. For the majority of military explosives such as HMX or TNT, their critical diameters are relatively small and they show minimal divergence from ideal performance over a large range of diameters [8]. For AN based explosives the d_c can be over 100 mm [9] and can still exhibit highly non-ideal behavior even at diameters in excess of a meter [10, 11]. The reason these explosives exhibit non-ideal

behavior in such a wide diameter range is due to their relatively long reaction zones caused by the low decomposition rate of AN [11]. A longer reaction zone allows for more lateral energy loss, leading to reduced shock sensitivity and a greater d_c [12]. A consequence of these larger critical diameters is that greater amounts of material are required to achieve steady detonation. This subsequently increases the time and cost of these experiments as well as necessitates facilities and equipment capable of larger scale detonation experiments.

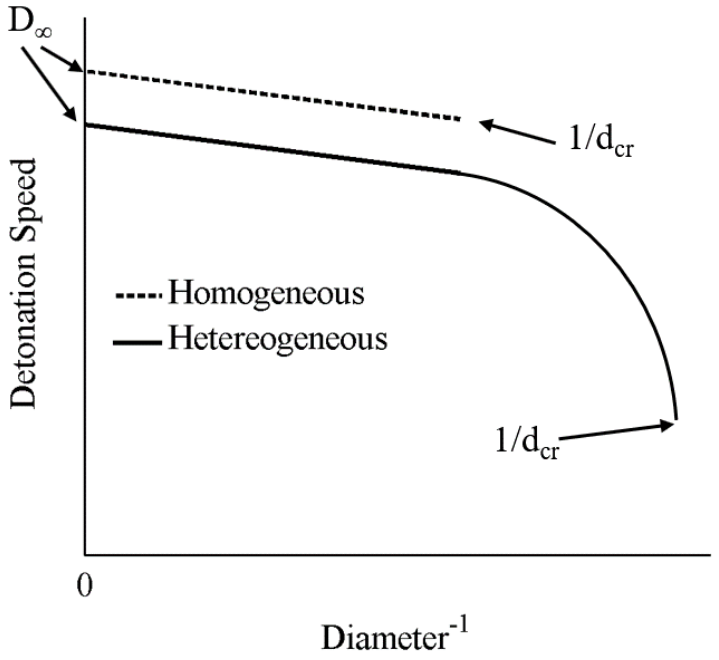

Fig. 1.1.: An example of a diameter effect curve for an explosive.

Shock sensitivity encompasses the threshold for initiation under transient shock conditions as well as the threshold for propagation of a steady detonatoin [13]. Because it is a property involving threshold conditions, the conditions for failure and initiation have long been used as metrics for the shock sensitivity of an explosive in forms such as critical diameter, gap, and run-to-detonation style tests. The initiation and failure regimes for detonation are similar as both are governed by the same competing phenomena. Both depend on how efficiently mechanical energy can be con-

verted to the thermal energy necessary for reaction and the ability of that reaction to produce chemical energy release in the time scale necessary to contribute to the shock front [14, 15]. In recent publications it was shown that reaction wave behavior in failing detonation events in overdriven sub-critical diameter charges could be correlated to the shock sensitivity of an explosive [16, 17]. In addition, it was shown that reactive flow models based on theory of ignition and growth can be calibrated using data from detonation failure events in sub-critical diameter charges [18]. The ability to characterize shock sensitivity using small-scale detonation failure experiments as well as use the transient data from such tests to calibrate models give this technique a lot of utility. These small-scale experiments could potentially augment or replace larger scale explosive tests. In Janesheski *et al.* [16], the run-to-failure distance (RTF) was used as the metric for the decay rate and was defined as the distance the reaction wave propagates through the charge until it decouples from the shock front. In Cummock *et al.* [17], the rate at which the velocity of the reaction wave decays (R_{UD}) as it propagates through the charge was used as the metric and was taken to be the average slope of the transient velocity curve. Note that term "detonation" implies a shock wave which is propagated by a steady reaction wave and as such does not apply to sub-critical diameter charges in which a steady detonation cannot be sustained. Therefore, these events are referred to as "failing detonations" and the term "reaction wave" is used in place of "detonation wave" to describe the ever-weakening area of chemical energy release behind the leading shock wave.

Using R_{UD} or RTF as a metrics for sensitivity not only offers a reduction in the amount of explosive material necessary as compared to critical diameter or gap type experiments, it also reduces the number of tests conducted. It eliminates the need for multiple sizes of attenuators or tube diameters. To further investigate the merit of this small-scale characterization technique and the relationship between failure rate and shock sensitivity, high speed imaging was used to determine transient velocity profiles for failing detonation events in various AN based explosives. The objectives of this work are threefold:

1. To further validate the small-scale method for shock sensitivity characterization that utilizes the failing detonation regime as described in Janesheski *et al.* [16] and Cummock *et al.* [17],

2. to present sensitivity data for various non-ideal explosive formulations involving ammonium nitrate (in particular for ANNM), and

3. to provide data sets from failing detonations in heterogeneous non-ideal explosive mixtures with known microstructure for the potential use of aiding modeling attempts.

In this work, transient reaction wave position and velocity profiles are used to compare the detonation failure behavior in small-scale (< 15 g), overdriven AN based explosive charges. Four different explosive systems, consisting of pure AN, ANFO, ANNM, and ANAl, were used to explore the effect of varying fuel type on the failure behavior. The effects of varying fuel percentage were also explored using ANNM and ANAl. ANFO and ANAl are both relatively well studied systems and were chosen as a means to compare the shock sensitivity results from this work to those available in the literature. In contrast, there is a scarcity of available data involving the detonation characteristics of ANNM, so characterizing its shock sensitivity was of particular interest. For each composition, the rate of decay of the reaction wave velocity was calculated. It is proposed that this decay rate can be correlated to the shock sensitivity of the explosive and be used to draw conclusions on mechanisms of initiation. Differences in decay rates and possible reasons for these differences are discussed.

2. EXPERIMENTAL METHODS

2.1 Experimental Configuration

All explosive charges in this study were pressed to a prescribed density inside of polyethylene terephthalate glycol (PETG) tubes with an inner diameter of 12.7 mm and a wall thickness of 1.59 mm. The inner diameter of the tubes must be large enough to allow for an adequate velocity decay rate for differentiation between compositions. If the tube diameters are too narrow, all of the initiated charges would fail shortly after the booster, providing minimal differences in R_{UD} for the different mixtures. The use of stronger confinement (i.e. metal tubes) would allow for smaller diameters; however, the use of imaging techniques such as those fielded here necessitates the use of transparent confinement. Quartz tubing was initially attempted, but the high acoustic velocity allowed the tube to shatter ahead of the reaction front, obstructing its view, in some lower velocity cases. There are other diagnostics which would allow for observation of the reaction wave in metal confinement, such as the microwave interferometry (MI) technique used in Cummock *et al.* [17]. However, the use of MI presented limitations as nitromethane (NM) was found to attenuate the microwave signal. Each charge was comprised of a 76.2 mm section of AN-based sample explosive boosted by a 19.05 mm section of donor explosive. The donor explosive was Primasheet® 1000 pressed to a density of 1.44 g/cm^3, representing 98% of the theoretical max density (TMD). The sample charge geometry is illustrated in Fig. 2.1. Detonation was initiated using an RP-502 Economy Exploding Bridgewire (EBW) detonator (Teledyne Risi). The detonation was contained within a thick-walled steel chamber. A Shimadzu Hypervision HPV-X2 high speed video camera was used to visualize the chemiluminescence of the reaction front in order to track its progression through the sample. This camera, capable of recording 256 frames

at 10 million frames per second, was focused on the sample charge through two 1.59 mm. polycarbonate shields. A fiducial image was recorded with the camera prior to capturing the detonation event. The triggering of the experiment was based on the electrical discharge from the firing unit to the detonator. A custom-built Hall effect sensor was used to sense current flow through the detonator wire.

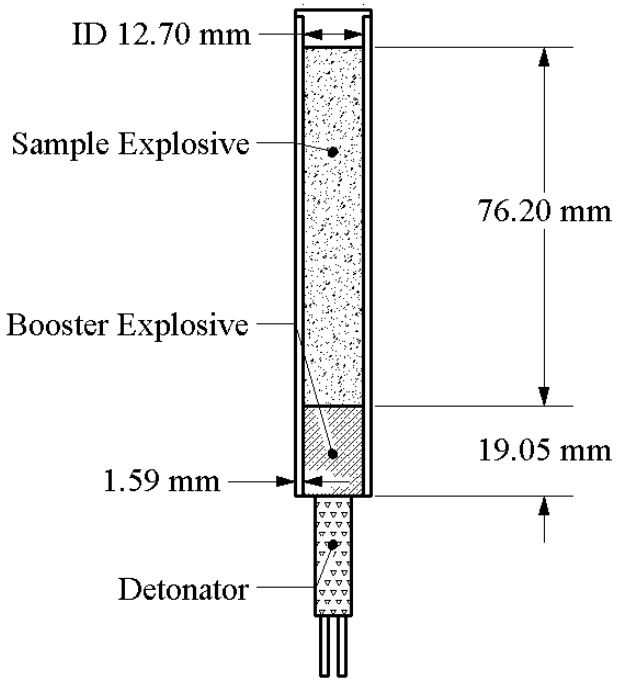

Fig. 2.1.: Details and dimensions of explosive charge.

2.2 Sample Preparation

The explosive charges in this work were all various HME mixtures comprised of ammonium nitrate and a fuel. The ammonium nitrate used was in the form of Kinepouch^{TM} (Orica Manufacturing Company). Kinepouch^{TM} is part of a binary mining explosive consisting of 97.1 wt.% ammonium nitrate and 2.9 wt.% glass microballoons (GMBs) for increased shock sensitivity when combined with nitromethane (the other component of the binary explosive). The mean particle diameters for the

ammonium nitrate and the microballoons are 60 μm and 50 μm, respectively [18]. The AN was place in a drying oven for 72 hours prior to mixing with fuel in order to reduce the moisture content. The fuels investigated were nitromethane, diesel fuel, and aluminum particles. The aluminum used was Al-100 (Atlantic Equipment Engineers), which is spherical in shape and has a diameter of 1-5 μm.

In order to achieve an intimate mixture between the fuel and oxidizer, all samples were mixed via a Resodyn LabRAM$^{\text{TM}}$ resonant mixer for 10 minutes at an intensity of 60% ($\sim$690 m/s^2). Due to the deliquescent nature of AN, precautions had to be taken to prevent it from absorbing atmospheric moisture. The critical relative humidity (CRH) of AN is 66.9% at 20°C. Above this relative humidity, AN will begin to rapidly absorb moisture from the atmosphere. Therefore, sample preparation was conducted when the relative humidity was below 60% [19]. After mixing, the samples were pressed to their target densities in eight increments of 9.53 mm, providing an increment aspect ratio of 0.75. This acted to minimize density gradients along the charge axis. All charges were capped and sealed after pressing and detonated within 24 hours. The details for each charge composition are listed in Table 2.1. With the exception of the ANFO mixture, the densities in Table 2.1 reflect a constant AN particle bed density of 0.96 g/cm^3 (55% of the TMD of Kinepouch$^{\text{TM}}$). This was designed so that the only change between charges is the type and percentage of fuel filling the interstitial voids in the AN (i.e. the volume percent of AN was held constant). This particle bed density was chosen such that it was above the tapped density of the Kinepouch$^{\text{TM}}$ ($\sim$0.90 g/cm^3) so that no further particle settling occurred. Note that the ANFO mixture consisting of 6 wt.% diesel (stoichiometric) has an AN particle bed density of 0.92 g/cm^3 (53% TMD of the Kinepouch$^{\text{TM}}$). For the mixtures containing NM as the fuel, 30 wt.% represents a nearly fully saturated mixture. It was found that the addition of NM beyond this weight percent resulted in separation from the particle bed during pressing such that the charge composition could not be accurately determined. Three charges for each composition were made

and detonated with the exception of ANNM20, ANNM25, and ANNM30, in which four charges were made and detonated.

Table 2.1.: Summary of charge compositions and properties. OB is the oxygen balance by mass and values for D_{CJ} were calculated using CHEETAH 7.0 [20].

Abbr.	Fuel	Fuel wt.%	OB (%)	Density (g/cm^3)	% TMD	D_{CJ} ($mm/\mu s$)
AN	-	-	19	0.96	55	4.39
ANFO	diesel	6	-2	1.02	63	5.54
ANNM5	nitromethane	5	16	1.01	60	4.79
ANNM10	nitromethane	10	14	1.07	65	5.20
ANNM15	nitromethane	15	11	1.13	70	5.63
ANNM20	nitromethane	20	8	1.2	76	6.10
ANNM25	nitromethane	25	5	1.28	83	6.61
ANNM30	nitromethane	30	2	1.37	92	7.21
ANAl5	aluminum	5	14	1.01	57	4.75
ANAl10	aluminum	10	9	1.07	59	4.97
ANAl15	aluminum	15	3	1.13	62	5.13
ANAl20	aluminum	20	-2	1.2	64	5.28

2.3 Data Analysis

Videos taken with the high-speed camera were used to track the reaction wave progress through each charge and produce position-time data that can be differentiated to produce transient velocity curves in order to determine rates of velocity decay. The image sequence in Fig. 2.2 taken from select frames of an ANNM20 sample showcases typical raw data gathered from the high-speed recordings. The lu-

minous region in each of the frames is taken to be the reaction front. Using Matlab®, the position of this front is tracked through each frame starting with the first frame in which the shock enters the sample explosive until the reaction dies out (light is no longer produced) or it reaches the end of the charge. In most cases this process can be automated. Each image in the sequence is binarized to create a single bit image showing just the luminous reaction front. The weighted centroid (based on location and the pixel intensity of the non-binarized image) of the region indicates the vertical position of the front. For some charges, particularly those involving aluminum as the fuel where reaction in the Taylor wave was often as bright as the front, the center of the luminous region was not representative of the position of the front. For these cases, the front position was selected manually. These selected points give the reaction front propagation distance over time. The resolution of the camera is limited to 400 pixels vertically, and since each shot is 76.2 mm long, the scale for each shot was $\sim$5 pixels/mm. At 10,000,000 fps, a shock velocity of 2-6 mm/μs can only progress 1-3 pixels per frame. Therefore, typical finite difference numerical differentiation of the position versus time data would not provide any useful information as all velocities would fall into one of three bins. To overcome this, a Fourier transformation data processing technique is used to both smooth and differentiate the shock position data [21–23]. This reduces the effects of discrete data and point selection error [23]. Using Matlab®, a Lagrangian polynomial is fitted to the first and last two data points and subtracted from the curve (see Fig. 2.3). The remainder, no zero-valued on the ends, has a quasi-periodic profile. A fast Fourier transformation (FFT) is performed on the remainder, producing a spectrum of its frequencies. As shown in Fig. 2.4, the frequency spectrum shows a large peak at low followed immediately by a downward trend until being intersected by a near-horizontal band which extends out to the higher frequencies. This initial peak contains the bulk of the signal, and the horizontal band beyond this represents the noise due to error inherent in discrete measurement. A low pass filter (2^{nd} order butterworth) is used to remove all frequencies after the initial downward trend in the frequency spectrum. By setting the cutoff frequency

too low, there is potential to cause severe distortion of the signal beyond that of noise rejection. The R^2 values for all filtered position curves as compared to their original data sets are 0.9998 or higher. This confirms that major frequency components of the true signal are not being removed along with the noise. After filtering, the frequency spectrum is multiplied by $j\omega$ to obtain the derivative in the frequency domain. It is then converted back into the time domain where it is added to the derivative of the subtracted polynomial to produce the velocity curve (see Fig. 2.5).

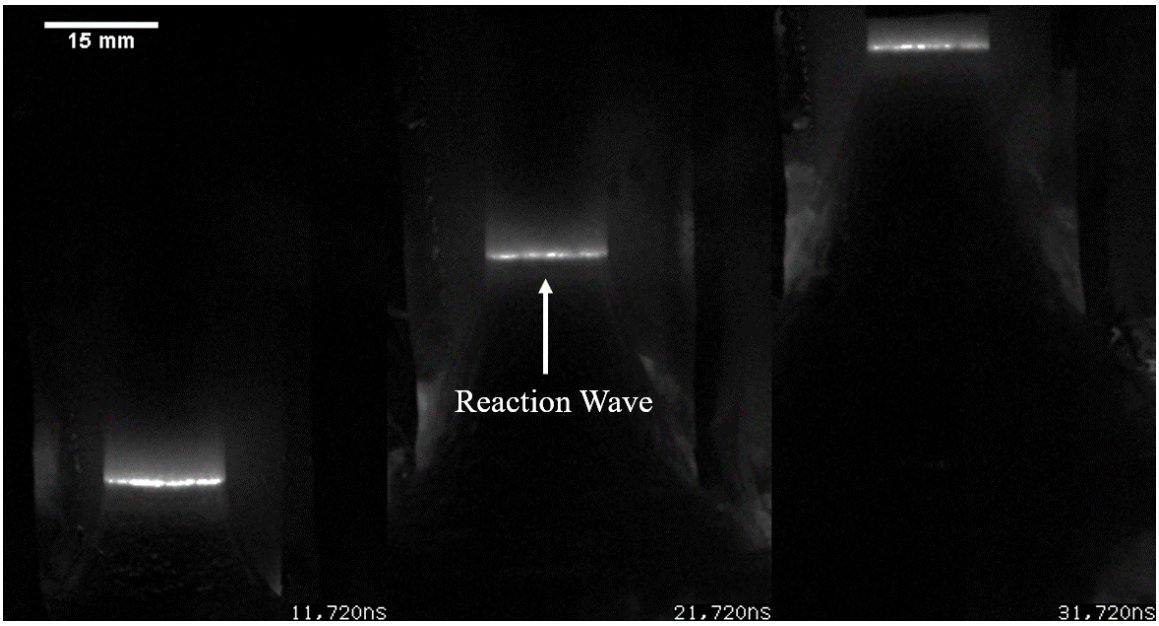

Fig. 2.2.: Sequence of frames taken from ANNM20 detonation event showing the progression of the reaction wave (luminous region).

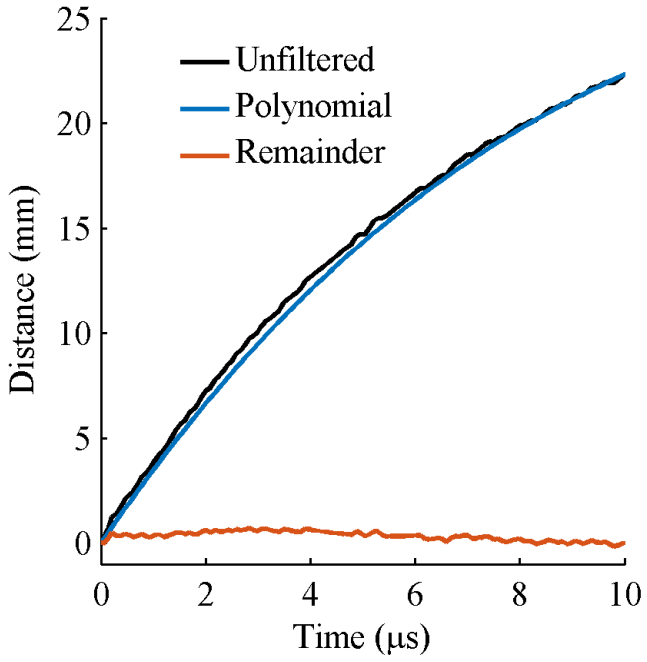

Fig. 2.3.: Position vs. time curve for AN with subtracted polynomial and remainder.

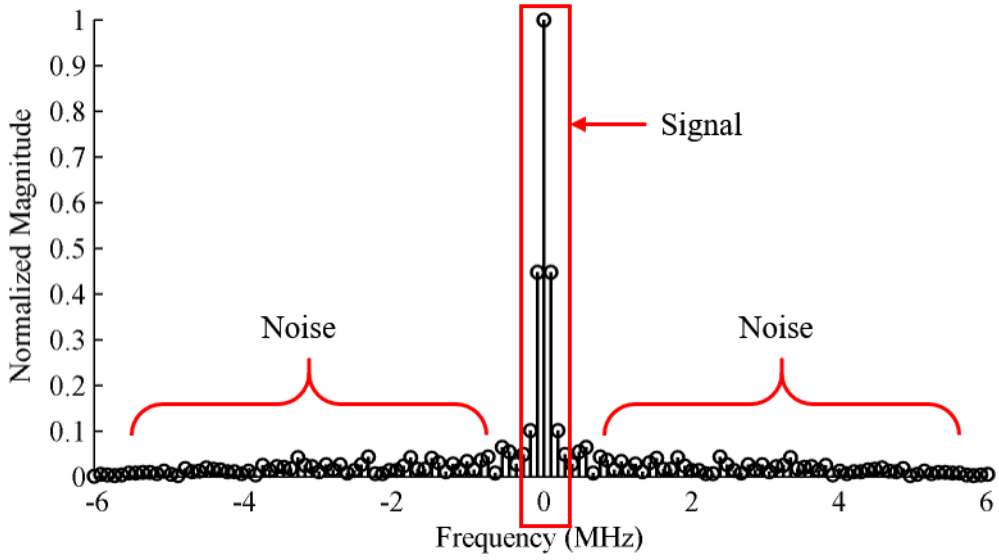

Fig. 2.4.: Frequency spectrum for AN remainder curve.

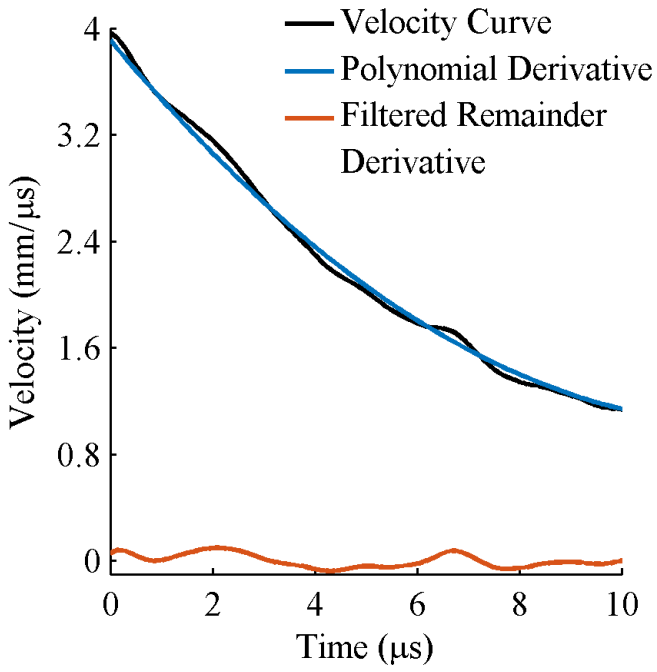

Fig. 2.5.: Reaction wave velocity vs. time curve for AN created from adding the derivative of the subtracted polynomial and the filtered remainder that was differentiated in the frequency domain.

The resultant transient velocity profiles are then used to determine the average rate of decay of the reaction velocity (R_{UD}). R_{UD} is determined by applying a linear fit to each velocity versus time curve (see Fig. 2.6). For the reactions that fail to propagate the length of the charge, the linear fit is applied from the first point at the booster-sample interface to the point at which the reaction ceases. The samples in which the reaction propagates the entire length of the charge (namely those containing 15-30 wt.% NM) are handled differently. These samples required anywhere between ~22-35 μs to reach the end of the charge length. Since it can be assumed that samples which reach the end of the charge would continue to propagate further, charges which take longer to complete the run would have an artificially higher amount of data points to fit across. It would be an unfit comparison to take the failure rate over the entire curve. Doing so would lead to the slowest charge having an artificially higher

or lower R_{UD} because it has a longer time interval and R_{UD} represents the average change in velocity over a finite time interval. In order to allow for fair comparison, the linear fit is taken from the moment it enters the sample charge to the time at which the fastest sample (ANNM25, which took 22.5 μs) finished the run.

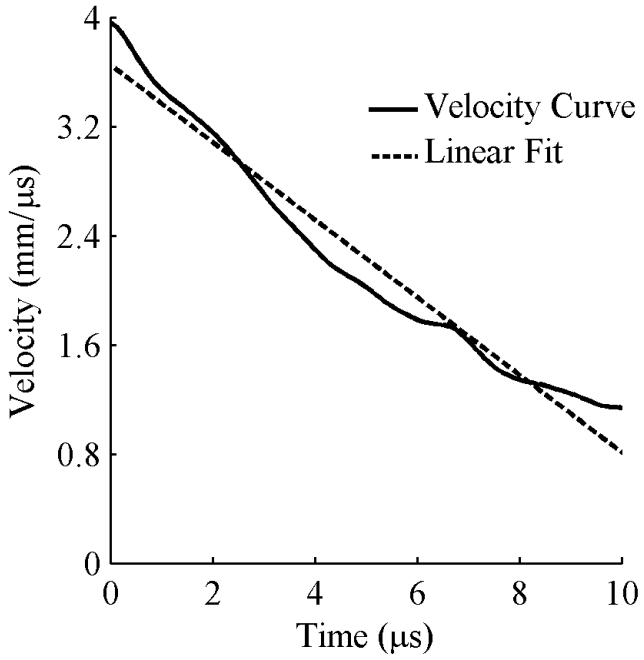

Fig. 2.6.: Linear fit of the velocity vs. time curve for AN to determine velocity decay rate.

3. RESULTS AND DISCUSSION

The absolute values of the average reaction wave velocity decay rates for each composition are shown in Fig. 3.1. Square points represent compositions in which the reaction wave propagated the entire length of the charge. Lower absolute decay rates correspond to higher shock sensitivity and vice versa. It is important to note that the quantitative value of $|R_{UD}|$ is of little significance; instead, it serves to provide information on the shock sensitivity of explosives relative to each other. This is because the numerical value for failure rate is highly dependent on the diameter and confinement of the charge. These average rates of decay were compared to their respective average RTF distances and published critical diameters for charges of similar compositions (see Table 3.1). Upon initial inspection, for the charges that failed to propagate the length of the charge, the $|R_{UD}|$ values are consistent with the distances at which the reactions ceased (see Fig. 3.2). The AN without any fuel additives exhibited the lowest sensitivity followed by ANFO with 6 wt.% fuel. This is consistent with studies involving compositions of comparable particle size and density which have reported a critical diameter greater than 127 mm for pure AN [24] and 77 mm for ANFO [25]. It can also be seen in Fig. 3.1 that ANNM5 and ANAl5 are more sensitive than ANFO despite having a similar mass of fuel and being less oxygen balanced. This is due to the greater thermodynamic state dependence of the AN and diesel reaction.

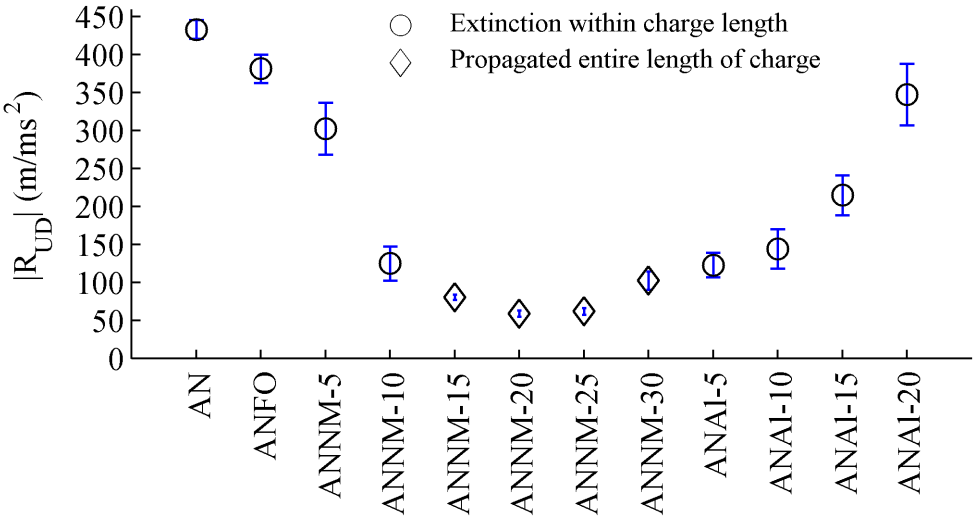

Fig. 3.1.: Absolute values of the average rate of reaction wave velocity decay ($|R_{UD}|$) and the standard deviations for each composition.

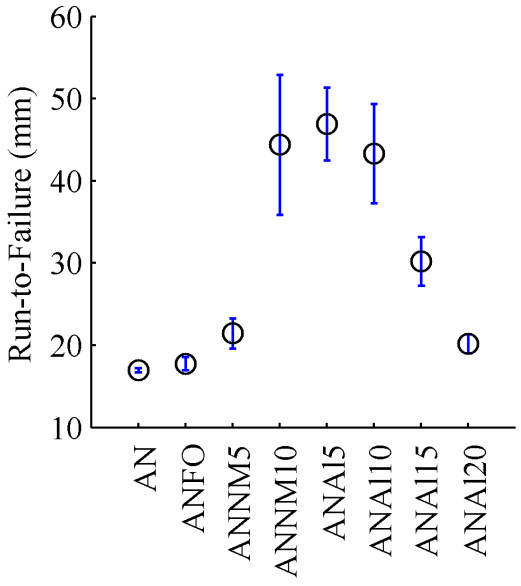

Fig. 3.2.: Run-to-failure (RTF) and standard deviations for each composition which failed within the length of the charge.

Table 3.1.: Average rate of velocity decay ($|R_{UD}|$) and run-to-failure (RTF) of each charge with published critical diameter data for charges of similar composition [24–26].

Composition	Average R_{UD} (m/ms^2)	Average RTF (mm)	d_c (mm)
AN	43	17	>127 [24]
ANFO	38	18	77 [25]
ANNM5	30	22	-
ANNM10	13	44	-
ANNM15	8	-	-
ANNM20	6	-	13<d<16 [26]
ANNM25	6	-	-
ANNM30	10	-	-
ANAl5	12	47	25 [24]
ANAl10	14	43	25 [24]
ANAl15	22	30	25 [24]
ANAl20	35	20	25<d<50 [24]

3.1 ANAl

For the aluminized AN compositions, the decay rates displayed in Fig. 3.1 indicate that maximum sensitivity occurs at 5 wt.% Al powder and decreases with further addition of Al. This is consistent with findings for similar ANAl compositions in which the addition of only 1 wt.% Al causes a significant reduction in d_c and this trend continues until reaching a minimum at around 8 wt.% Al [24,27,28]. After this point, the critical diameter increases with additional aluminum. Even at 20 wt.% Al, the $|R_{UD}|$ was less than that of ANFO. This is in agreement with studies done by Cook *et al.* [24] in which the critical diameter of AN containing 20 wt.% Al was

between 25 and 50 mm. Similar to ANNM, maximum shock sensitivity in ANAl (as indicated by the minimum $|R_{UD}|$) occurs before a stoichiometric mixture ($\sim$18 wt.% Al) is achieved.

The reaction rate of AN and Al is dominated by mass diffusion and heat conduction [27]. The ignition delay time for AN is considerably lower than that of the Al due to the high thermal activation requirements of metal particles. The AN particles begin decomposition first through inward grain burning which influenced by the specific surface area of AN available for hot spot igniton [27]. The reaction of aluminum particles is dependent on the reaction zone temperature, particle size, and the availability of the oxidative decomposition species of AN [29]. For a given temperature, particle size, and oxygen balance, only a given percentage of the aluminum can be expected to react within the reaction zone. It can be seen in Fig. 3.3 that even at 5 wt.% Al a significant portion of the oxidation is taking place in the detonation products behind the sonic plane. The addition of any aluminum beyond this will only act as a thermal ballast within the reaction zone [30]. Furthermore, additional aluminum reduces the amount of void spaces (which act as hot spots) and the available surface area of AN for hot spot ignition.

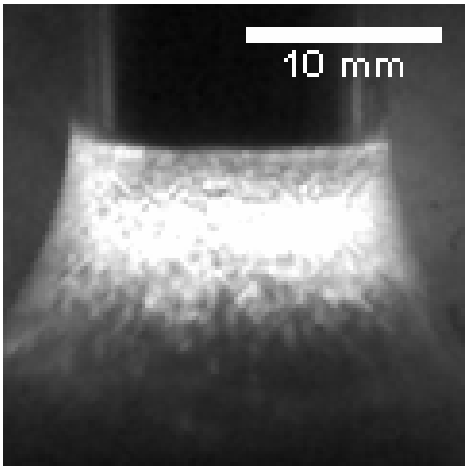

Fig. 3.3.: Afterburning of aluminum (indicated by light emission) in post detonation products of ANAl5.

3.2 ANNM

Looking at the $|R_{UD}|$ for mixtures containing NM, sensitivity rises with NM content until hitting a peak at 20-25 wt.% at which point it begins to become less sensitive. Since an oxygen balanced mixture of AN and NM occurs at ∼32 wt.%, this trend is not solely due to stoichiometry. Instead, this reflects an interplay between hot spot density and stoichiometry. Since all charges had the same particle bed of AN, as fuel percentage increases the volume of interstitial voids decreases. Sensitivity initially increases as the composition gets closer to a stoichiometric mixture. As the bed becomes increasingly saturated, there is a reduction in the void space which act as more efficient hot spots than the impedance mismatch between AN and NM [31]. As the initial specific surface of ignited hot spots is reduced it becomes increasingly difficult for them to coalesce and consume the explosive material on the time scale necessary. Eventually, the benefits of improved oxygen balance are outweighed by the reduction in energy release within the reaction zone. As a result, at 30 wt.% NM the reaction wave velocity begins to decay more rapidly as shown in Fig. 3.4. In the high-speed videos, the luminous region of the reaction zone for ANNM30 can be seen to become sporadic due to the lower amount of less uniformly distributed hot spots (see Fig. 3.5). Charge compositions with a fully saturated particle bed were attempted, but results could not be obtained from them due to difficulties in charge composition consistency and optically tracking the reaction front. After initiation, the reaction zone in these saturated charges would periodically cease chemiluminescence and then faintly reinitiate as the leading shock interacted with a hot spot (most likely provided by the GMBs present in the Kinepouch^{TM}). Unlike those containing 15-30 wt.% NM, none of the fully saturated compositions propagated the full charge length indicating further decreased sensitivity.

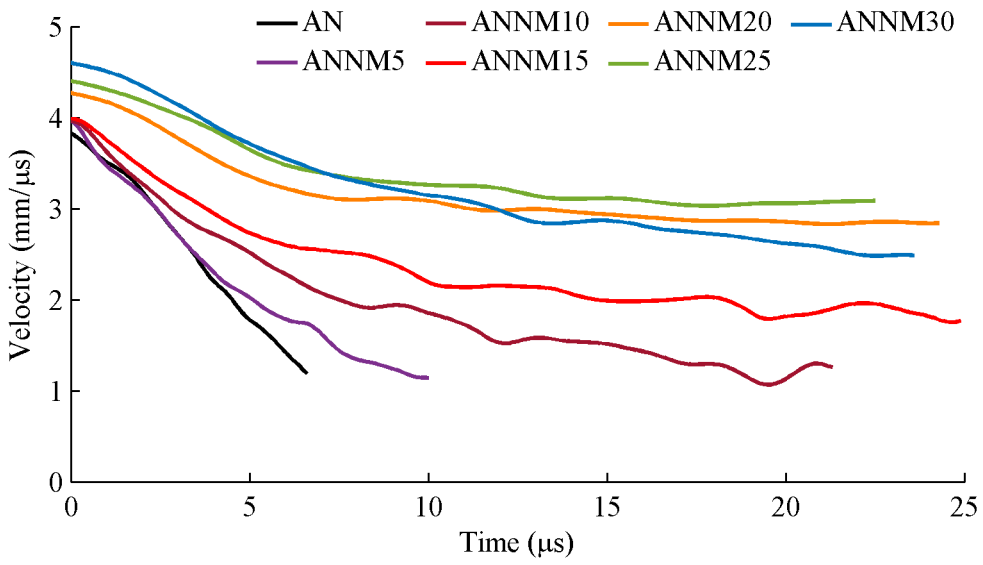

Fig. 3.4.: Transient reaction wave velocity curves for AN containing 0-30 wt.% fuel.

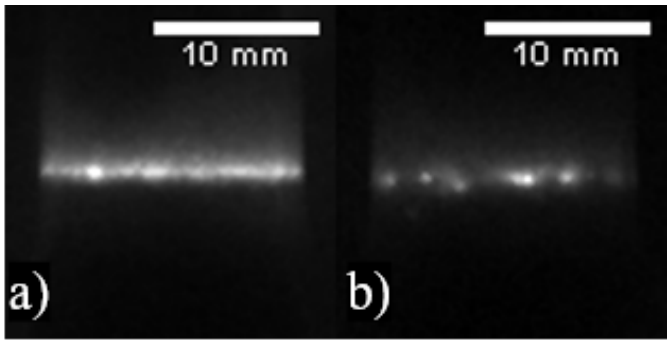

Fig. 3.5.: Images of the reaction zones for a) ANNM30 and b) ANNM25.

Work done by Souers *et al.* [26] demonstrated that a charge of ANNM with a similar composition to that of ANNM20 failed to yield a steady detonation at a diameter of 12.78 mm. Since ANNM20 was the most sensitive ANNM composition (along with ANNM25 which had an equivalent $|R_{UD}|$), this should indicate that all the charges tested in this work failed to produce a steady detonation. However, from Fig. 3.4, ANNM15-30 seem to assymptote out to a nearly steady velocity (for ANNM30

some of the velocity curves still displayed some downward trend toward the end of the run due to the sporadic nature of the reaction wave). Due to the charge length used, it is uncertain whether or not ANNM15 – ANNM30 are failing and may in fact be above their critical diameter. Dividing these settling velocities (taken as the average velocity of the last 10% of each curve) by their respective CJ velocity reveal the same trend as the decay rate. As seen in Fig. 3.6, ANNM20 and ANNM25 reach nearly identical $\%D_{CJ}$, followed by ANNM15 and then ANNM30. From Cooper [32], the detonation velocity versus charge radius relationship can be approximated with the following correlation equation:

$$(D/D_\infty) = 1 - A_R/r \tag{3.1}$$

where D is the detonation velocity, D_∞ is the infinite diameter detonation velocity, A_R is the rate coefficient constant which is different for different explosives, and r is the charge radius. In this work it was shown that the rate coefficient A_R can be correlated to the critical radius r_c with higher A_R denoting a higher r_c. Using Eq. (3.1) the average rate coefficients for ANNM15-30 were calculated. These values which are displayed in Fig. 3.6 are 4.3, 3.5, 3.5, and 4.4 corresponding to 15%, 20%, 25%, and 30% NM respectively.

Charges consisting of neat nitromethane were also attempted, but no reaction zone was observed. Instead, a region of faint luminosity starting at the initiation plane propagated forward with a decreasing cross section, forming a parabolic shape up to a point at which all chemiluminescence ceased. The critical diameter for neat nitromethane is 16.2 cm [33] which is much smaller than some of the other compositions, but this is not reflected by the decay rate. This might be expected since the conformation of the diameter effect curve for homogeneous explosives such as neat NM is different than that of heterogeneous explosives [33]. As was shown in Fig. 1.1, homogeneous explosives have linear diameter effect curves that have minimal velocity deficit from D_∞ at d_c. In addition, initiation in such explosives does not occur immediately behind the leading shock wave and instead occurs after some induction time once compression of the bulk medium has provided enough heating for thermal

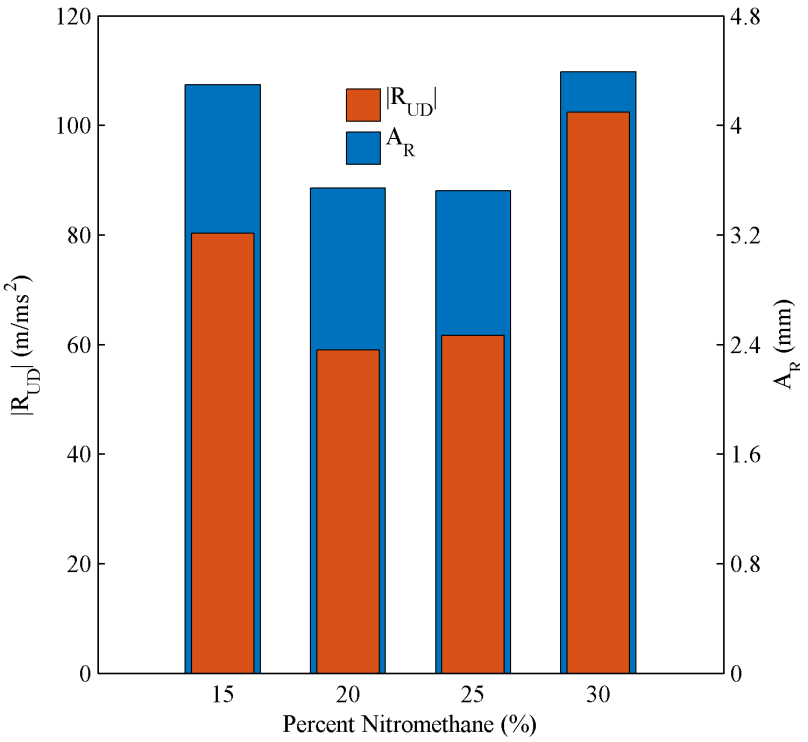

Fig. 3.6.: Rate of velocity decay (R_{UD}) for charges which propagated the length of the charge (left axis) and corresponding rate coefficient (A_R) values calculated using Eq. (3.1) (right axis).

explosion to occur [31]. In contrast, the diameter effect curves for heterogenous explosives exhibit a concave downward region near the d_c which can have relatively large velocity deficits from D_∞ [33]. Initiation in these explosives occurs almost immediately behind the leading shockwave [31]. It was postulated by Engelke [33] that the linear region of heterogenous diameter effect curves represent a regime where both heterogeneous (hot spots) and homogeneous (bulk shock heating) mechanisms play a role in the energy release rate. The concave region of the diameter effect curve for heterogeneous explosives therefore represents a regime where the thermodynamic state within the reaction zone is not sufficient for bulk shock heating to contribute to energy release and heterogeneous mechanisms dominate. In equations for steady det-

onation developed by Engelke and Bdzil [34] it was shown that the state dependence of the heat release rate is considerably less for heterogeneous mixtures involving NM than it was for homogeneous NM. This dual mechanism idea was later expounded upon by Dremin [35] who developed the concept of a characteristic shock compression P^*. This P^* is roughly equal to the critical pressure of detonation initiation for explosives at maximum density (i.e. no porosity). For shock pressures above P^*, homogeneous mechanisms dominate and charge structure plays little role in propagation of the detonation. For shock pressures below P^*, heterogeneous mechanisms dominate. The shock wave pressure at the central axis is always above P^* for charges above failure diameter; however, in curved detonation fronts the shock pressure is not constant due to the effects of rarefaction waves. At sufficient diameters, the curvature from rarefaction losses is minimal such that the majority of the detonation front is above P^*. As diameter decreases the effect of these losses becomes more pronounced and this ratio reverses. For charges near or below their critical diameter, such as those investigated in this work, it can be said that heterogeneous initiation mechanisms dominate and the critical pressure for detonation initiation for maximum density explosives is not achieved in the majority of the detonation front. The implication of this is that this technique for sensitivity characterization is only applicable for heterogeneous explosives.

4. SUMMARY AND CONCLUSIONS

Small-scale experiments utilizing sub-critical diameter charges were conducted to determine the effects of fuel type and percentage on the shock sensitivity of various ammonium nitrate based explosives (AN, ANFO, ANAl, and ANNM). Using high speed imaging, the reaction wave propagation was recorded and analyzed to determine rate of velocity decay (R_{UD}) as a metric for sensitivity. All mixtures of ANNM and ANAl showed greater shock sensitivity that AN and ANFO. It was determined that maximum sensitivity for both ANNM and ANAl occurred at fuel percentages below an oxygen balanced composition. For ANNM it was postulated that it was due to an interplay between stoichiometry of the mixture and the density of hot spots due to porosity in an increasingly saturated particle bed. In the case of ANAl, it would seem the trend is due to the lack of conversion of aluminum within the reaction zone. Additional aluminum acts as a thermal ballast as well as decreases the available specific surface area of AN particles for hot spot ignition. The run-to-failure (RTF) distance for samples which failed to propagate the length of the charge was also used as a sensitivity metric and aligned with the R_{UD} trends. For AN, ANFO, and ANAl the shock sensitivity results show good agreement with published critical diameter values. There is a paucity of available shock sensitivity data for ANNM with which to compare. In lieu of critical diameter data, calculated reaction rate coefficients from Cooper's [32] (which are correlated to critical radius) lend credibility to the results.

This work builds upon and helps to validate previous observations [16,17] that the rate at which reaction wave velocity decays in charges at or near their critical diameters can be used a measure of shock sensitivity. This method can be implemented rapidly using minimal material in order to investigate the wide parameter space associated with highly non-ideal explosive systems; in addition, the transient velocity data can be used to calibrate models which could alleviate the need for more costly

large-scale tests in some cases. However, large-scale tests should be conducted to address the scalabilty of the results from this type of analysis. Future studies are needed to investigate if the R_{UD} values, which in this case only provided relative sensitivity information, can be used to develop more quantitative correlations. Such correlations would likely be extremely sensitive to the nature and diameter of confinement.

REFERENCES

REFERENCES

[1] T. Levdikova, "Ammonium nitrate (an): 2014 world market outlook and forecast up to 2018," Jan 2014. [Online]. Available: https://www.prweb.com/releases/2014/02/prweb11538735.htm

[2] J. M. Modak and J. M. Modak, "Haber process for ammonia synthesis," *Resonance*, vol. 7, no. 09, 2002.

[3] W. Pittman, Z. Han, B. Harding, C. Rosas, J. Jiang, A. Pineda, and M. S. Mannan, "Lessons to be learned from an analysis of ammonium nitrate disasters in the last 100 years," *Journal of hazardous materials*, vol. 280, pp. 472–477, 2014.

[4] National Consortium for the Study of Terrorism and Responses to Terrorism (START), "Global terrorism database," web, 2018.

[5] *Terror Operations: Case Studies in Terrorism*, ser. DCSINT Handbook. US Army Training and Doctrine Command, August 2005, no. 1.01.

[6] *Homemade Explosives*, 3rd ed. Defense Intelligence Agency, July 2014.

[7] Y. Horie, Ed., *Shock Wave Science and Technology Reference Library.* Springer, 2009, vol. 3.

[8] Z. Fan, Ed., *Shock Wave Science and Technology Reference Library.* Springer, 2009, vol. 4.

[9] M. A. Cook, "Explosives—a survey of technical advances," *Industrial & Engineering Chemistry*, vol. 60, no. 7, pp. 44–55, 1968.

[10] P. W. Cooper, *Explosives Engineering.* VCH Publications, New York, 1996.

[11] A. Miyake, Y. Ohtagaki, T. Abe, Y. Wada, Y. Nakayama, and T. Ogawa, "Experimental determination of the detonation front curvature of non-ideal explosive anfo," in *Materials Science Forum*, vol. 465. Trans Tech Publ, 2004, pp. 181–184.

[12] Z. Fan, Ed., *Shock Wave Science and Technology Reference Library.* Springer, 2009, vol. 4.

[13] D. Price, "Shock sensitivity, a property of many aspects," NAVAL ORDNANCE LAB WHITE OAK MD, Tech. Rep. NOLTR-70-73, 1970.

[14] H. Eyring, R. E. Powell, G. H. Duffy, and R. B. Parlin, "The stability of detonation." *Chemical Reviews*, vol. 45, no. 1, pp. 69–181, 1949. [Online]. Available: https://doi.org/10.1021/cr60140a002

[15] J. E. Field, N. K. Bourne, S. J. P. Palmer, S. M. Walley, J. M. Smallwood, J. E. Field, and P. Gray, "Hot-spot ignition mechanisms for explosives and propellants," *Philosophical Transactions of the Royal Society of London. Series A: Physical and Engineering Sciences*, vol. 339, no. 1654, pp. 269–283, 1992. [Online]. Available: https://royalsocietypublishing.org/doi/abs/10.1098/rsta.1992.0034

[16] R. S. Janesheski, L. J. Groven, and S. F. Son, "Detonation failure characterization of homemade explosives," *Propellants, Explosives, Pyrotechnics*, vol. 39, no. 4, pp. 609–616, 2014. [Online]. Available: https://onlinelibrary.wiley.com/doi/abs/10.1002/prep.201300041

[17] N. R. Cummock, J. Jesus O. Mares, I. E. Gunduz, and S. F. Son, "Relating a small-scale shock sensitivity experiment to large-scale failure diameter in an aluminized ammonium nitrate non-ideal explosive," *Combustion and Flame*, vol. 194, pp. 271 – 277, 2018. [Online]. Available: http://www.sciencedirect.com/science/article/pii/S0010218018302037

[18] D. E. Kittell, N. R. Cummock, and S. F. Son, "Reactive flow modeling of small scale detonation failure experiments for a baseline non-ideal explosive," *Journal of Applied Physics*, vol. 120, no. 6, p. 064901, 2016. [Online]. Available: https://doi.org/10.1063/1.4959818

[19] European Fertilizer Manufacturers Association, "Guidance for the storage, handling and transportation of solid mineral fertilizers," Ave. E. van Nieuwenhuyse 4, B-1160 Brussels, Belgium, 2007.

[20] S. Bastea, L. E. Fried, K. R. Glaesemann, W. M. Howard, I. W. Kuo, P. C. Souers, and P. A. Vitello, *Cheetah 7.0 User's Manual*, Lawrence Livermore National Laboratory, Livermore, CA, USA, 2012, lLNL-SM-599073.

[21] G. Horlick, "Digital data handling of spectra utilizing fourier transformations," *Analytical Chemistry*, vol. 44, no. 6, pp. 943–947, 1972, pMID: 22384876. [Online]. Available: https://doi.org/10.1021/ac60314a014

[22] J. W. Hayes, D. E. Glover, D. E. Smith, and M. W. Overton, "Some observations on digital smoothing of electroanalytical data based on the fourier transformation," *Analytical Chemistry*, vol. 45, no. 2, pp. 277–284, 1973. [Online]. Available: https://doi.org/10.1021/ac60324a022

[23] R. De Levie, S. Sarangapani, and P. Czekaj, "Numerical differentiation by fourier transformation as applied to electrochemical interfacial tension data," *Analytical Chemistry*, vol. 50, no. 1, pp. 110–115, 1978.

[24] M. A. Cook, A. S. Filler, R. T. Keyes, W. S. Partridge, and W. Ursenbach, "Aluminized explosives," *The Journal of Physical Chemistry*, vol. 61, no. 2, pp. 189–196, 1957.

[25] R. A. Catanach and L. G. Hill, "Diameter effect curve and detonation front curvature measurements for anfo," *AIP Conference Proceedings*, vol. 620, no. 1, pp. 906–909, 2002. [Online]. Available: https://aip.scitation.org/doi/abs/10.1063/1.1483684

[26] P. C. Souers, L. Lauderbach, K. Moua, and R. Garza, "Size effect and cylinder test on several commercial explosives," in *AIP Conference Proceedings*, vol. 1426, no. 1. AIP, 2012, pp. 343–346.

[27] B. Khasainov, B. Ermolaev, H. Presles, and P. Vidal, "Numerical modeling of non-ideal detonations in ammonium nitrate/aluminium mixtures and their blast effect," in *Twelfth Symposium (International) on Detonation*, 2002, pp. 296–302.

[28] B. Zygmunt, "Detonation parameters of mixtures containing ammonium nitrate and aluminium," *Central European Journal of Energetic Materials*, vol. 6, no. 1, pp. 57–66, 2009.

[29] G. A. Leiper and J. Cooper, "Reaction of aluminium and ammonium nitrate in nonideal heterogeneous explosives," in *Tenth Symposium (International) on Detonation*, 1993, pp. 267–275.

[30] A. Maranda, "Research on the process of detonation of explosive mixtures of the oxidizer fuel type containing aluminium powder," *Propellants, Explosives, Pyrotechnics*, vol. 15, no. 4, pp. 161–165, 1990.

[31] D. M. Dattelbaum, S. A. Sheffield, D. B. Stahl, A. M. Dattelbaum, W. Trott, and R. Engelke, "Influence of hot spot features on the initiation characteristics of heterogeneous nitromethane," in *Fourteenth Symposium (International) on Detonation*, 2010, pp. 11–16.

[32] P. Cooper, "A new look at the run distance correlation and its relationship to other non-steady state detonation phenomena," in *Tenth Symposium (International) on Detonation*, 1993, pp. 386–393.

[33] R. Engelke, "Effect of a chemical inhomogeneity on steady-state detonation velocity," *The Physics of Fluids*, vol. 23, no. 5, pp. 875–880, 1980.

[34] R. Engelke and J. B. Bdzil, "A study of the steady-state reaction-zone structure of a homogeneous and a heterogeneous explosive," *The Physics of Fluids*, vol. 26, no. 5, pp. 1210–1221, 1983.

[35] A. N. Dremin, *Toward detonation theory*. Springer Science & Business Media, 1999.